

Internal acoustic resonances: small scattering center compared with the wavelength

Naruna E. Rodrigues, Gilberto Nakamura, and Odemir M. Bruno

Instituto de Física de São Carlos, Universidade de São Paulo, São Carlos 13566-590, Brazil

José Renato Alcarás and Alexandre S. Martinez

*Faculdade de Filosofia, Ciências e Letras de Ribeirão Preto,
Universidade de São Paulo, Ribeirão Preto 14040-900, Brazil*

In fields such as acoustics, electromagnetism, and quantum physics, the scattering of waves by localized objects is a fundamental phenomenon. Building on this, the present study investigates the energy distribution within a spherical scattering center during its interaction with an incident acoustic wave. The analysis reveals unexpected resonance effects driven by impedance mismatches between the scattering center and the surrounding ideal fluid. These resonance phenomena occur even when the magnitude order of the incident wavelength is significantly larger compared to the size of the scattering center. Such resonance behavior, observed in the small-particle regime, has potential applications in ultrasound imaging, targeted drug delivery, and metamaterial design.

I. INTRODUCTION

Wave scattering by localized objects (scattering centers) has been widely studied across fields such as acoustics, electromagnetism, classical mechanics, quantum physics, and particle theory [1]. The ongoing interest in scattering phenomena arises from their dual nature: the direct problem, which predicts scattering patterns based on the properties of the incident wave and the object, and the inverse problem, which determines the characteristics of the scattering centers from observed patterns [1]. This balance between prediction and deduction keeps scattering theory relevant in diverse applications. The origins of scattering research can be traced back to studies of acoustic phenomena, especially in naval engineering, where issues such as bursting air bubbles led to erosion and cavitation in propellers [2]. Rayleigh's groundbreaking work on bubble dynamics [3] opened the door to significant advancements in the field, enabling later research into bubble vibration modes [4], acoustic luminescence [5], and broader applications in acoustic metamaterials [6, 7], medical diagnostics [8, 9], and virus inactivation [10]. These developments highlight the wide-reaching impact of acoustic scattering, from industrial to biomedical applications.

Building on these foundations, Anderson's 1950 study on sound scattering by fluid spheres [11, 12] established the basis for research on more complex geometries, including cylinders [13], solid objects [14], and core-shell systems made from elastic and viscoelastic materials [15–17]. More recent findings reveal that materials like rubber silicones behave as fluid-like scattering centers due to their slow longitudinal sound propagation and negligible shear wave velocity when submerged in water [18, 19].

This behavior has practical implications for designing underwater isolation materials, with applications in submarines and naval vessels [20, 21]. In parallel with these practical advancements, theoretical progress has deepened our understanding of wave scattering across various media. The analysis of wave scattering involves key quantities such as energy and momentum transfer [22]. In elastic materials, energy storage is computed through the scalar product of displacement and traction vectors, while in fluids, pressure, and velocity waves are derived from scalar potentials, simplifying the analysis. Recent techniques proposed by Müller et al. [23] have drawn analogies between acoustic and electromagnetic scattering, expanding the theoretical framework and enhancing the analysis of wave interactions across multiple fields.

In contrast, acoustic scattering by small scattering centers (particles) compared with wavelength was often neglected due to their limited impact on direct wave propagation. Nevertheless, these particles can significantly affect energy transfer through mechanisms like Rayleigh scattering, which may either enhance or disrupt system performance [16, 24]. Accurately accounting for these effects is crucial, especially in applications requiring precise control, such as noise reduction, imaging technologies, and wave manipulation [25]. This study highlights the importance of addressing even minor scattering effects to improve overall system efficiency and reliability. Expanding the traditional concept of acoustic scattering, where an incident wave interacts with a scattering center, this research focuses on the dynamics of the wave that penetrates the scattering center. This study has already been addressed in optics with the finding of resonances and other related effects [26–31].

This internal wave, influenced by the internal scatter-

ing coefficient, exhibits divergences under specific combinations of media and the size of the scattering center. Moreover, analytical expressions for energy transfer in the small-particle regime are derived and validated through practical examples using media such as air, petrol, and water. In one case, resonance is observed inside the scattering center due to a significant impedance mismatch between the medium and the scattering center. This article is structured as follows. In Sec. II, we present the scattering process of acoustic waves by a small fluid sphere in spherical geometry. The analytical expressions derived for the energy transferred during single scattering events. In Sec. III, we calculate the energy distribution within the fluid sphere for different media, such as air, petrol, and water. Resonances may occur even when the scatterer is much smaller than the wavelength of the incident wave, which is not expected. These resonance peaks, driven by the impedance mismatch between the scatterer and the surrounding fluid, lead to substantial energy storage, highlighting the importance of addressing even minor scattering effects to improve system efficiency and reliability. Finally, in Sec. IV, our study provides a foundation for further investigations into more complex scattering geometries, such as core-shell structures, where interactions between materials could enhance energy localization and control.

II. ACOUSTIC WAVE SCATTERING BY A SPHERICAL PARTICLE

The propagation of harmonic acoustic waves in an ideal fluid with density ρ_0 is analyzed, following the formalism of Anderson and Faran [14, 32]. Since the acoustic waves are treated as small perturbations, the governing fluid equations are simplified through linearization. The wave propagates through the medium in an adiabatic manner, and the fluid is assumed to be irrotational. Under these conditions, both the pressure and velocity fields are derived from a scalar potential $\varphi(\mathbf{r})$ [33], which satisfies the Helmholtz equation $(\nabla^2 + k^2)\varphi(\mathbf{r}) = 0$, where k is the wave number, related to the angular frequency ω by $k = \omega/c$, with c being the speed of sound in the fluid [34]. This scalar potential governs the spatial behavior of the perturbations in the homogeneous fluid. The pressure field, $p(\mathbf{r}, t) = -\rho_0 \partial_t [e^{-i\omega t} \varphi(\mathbf{r})]$, represents the compression and rarefaction of the fluid as the wave propagates. The velocity field, $\mathbf{v}(\mathbf{r}, t) = e^{-i\omega t} \nabla \varphi(\mathbf{r})$, describes the oscillatory motion of fluid particles caused by the wave.

In addition, a spherical scattering center, which is also a fluid with radius a and density ρ_1 (where $\rho_1 \neq \rho_0$),

is now incorporated into the system and is positioned at the origin of the coordinate system. The incident acoustic wave, represented by the potential $\varphi_{\text{inc}}(\mathbf{r})$, interacts with the scattering center as it propagates through the surrounding fluid. Inside the scattering center, the acoustic field is described by a scalar potential $\varphi_1(\mathbf{r})$, while the scattered wave outside is represented by $\varphi_{\text{sc}}(\mathbf{r})$. All the presented potentials satisfy the Helmholtz equation, as both the fluid and the scattering center are assumed to be acoustically isotropic, supporting only longitudinal compressional waves. At the surface of the scattering center, the boundary conditions ensure the continuity of physical quantities across the interface between the scattering center and the surrounding fluid, taking into account the chosen geometry [34]. These conditions are, at $r = a$,

$$\rho_0(\varphi_{\text{inc}} + \varphi_{\text{sc}}) = \rho_1 \varphi_1, \quad (1a)$$

$$\frac{\partial}{\partial r}(\varphi_{\text{inc}} + \varphi_{\text{sc}}) = \frac{\partial \varphi_1}{\partial r}. \quad (1b)$$

The first boundary condition ensures that the pressure inside the scattering center matches the pressure in the surrounding fluid at the surface $r = a$. The second boundary condition requires continuity of the normal component of the velocity field, ensuring that the velocity of fluid particles at the surface is consistent between the two fluids, inside and outside the scattering center [33, 34]. In this context, it is assumed that the incident wave is plane and monochromatic, so the incident wave equation is written as:

$$\varphi_{\text{inc}}(k_0 r, \cos \theta) = B \sum_{\ell=0}^{\infty} (2\ell + 1) i^\ell j_\ell(k_0 r) P_\ell(\cos \theta), \quad (2a)$$

$$\varphi_1(k_1 r, \cos \theta) = B \sum_{\ell=0}^{\infty} b_\ell (2\ell + 1) i^\ell j_\ell(k_1 r) P_\ell(\cos \theta), \quad (2b)$$

$$\varphi_{\text{sc}}(k_0 r, \cos \theta) = B \sum_{\ell=0}^{\infty} s_\ell (2\ell + 1) i^\ell h_\ell^{(1)}(k_0 r) P_\ell(\cos \theta). \quad (2c)$$

In Eq. (2a), the incident wave φ_{inc} is expanded in spherical harmonics, where B represents the wave amplitude, and k_0 is the wave number in the surrounding fluid. The radial and angular components are captured by the spherical Bessel functions $j_\ell(z)$ and the Legendre polynomials $P_\ell(\cos \theta)$, respectively [35]. Since the wave inside the sphere retains the same modal decomposition as the incident wave, the internal wave in the scattering center is written similarly in Eq. (2b), with the coefficient b_ℓ representing the internal scattering strength. The spher-

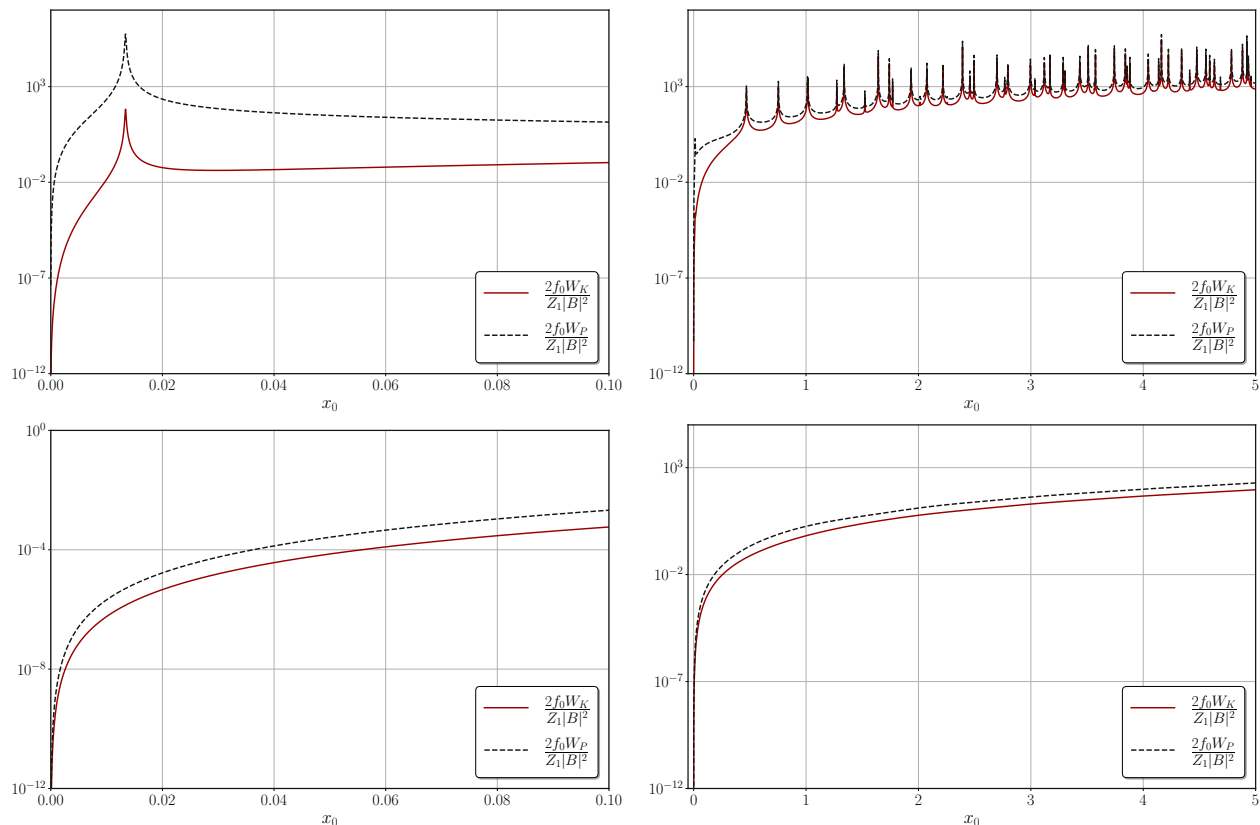


FIG. 1. Potential and kinetic energies as functions of the dimensionless size parameter x_0 for air (top) and petrol (bottom) in seawater. (top left) Small spherical scatterers resonate with incident acoustic waves at low impedance ratio, with potential energy dominating at low x_0 by several orders of magnitude. In contrast, (bottom left) the moderate impedance ration in petrol-seawater fail to support resonances entirely.

ical Bessel functions ensure regularity at the origin. Finally, Eq. (2c) describes the scattered wave, where spherical Hankel functions of the first kind, $h_\ell^{(1)}(k_0 r)$, represent outgoing waves at large distances, and the scattering coefficient s_ℓ governs the amplitude of the scattered wave [35].

One important concept is acoustic impedance, $Z = \rho c$, that measures the resistance a medium offers to sound waves, where c is the speed of sound. The impedance ratio between the two media, $m_t = Z_0/Z_1$, plays a key role in determining how much of the incident wave is reflected or transmitted at the boundary. For simplicity, the parameters $x_0 = k_0 a$ and $x_1 = k_1 a = m x_0$ (where $m = c_0/c_1$) are defined. This simplification streamlines the notation, making it easier to calculate the coefficients b_ℓ and s_ℓ using the boundary conditions Eqs. (1a–1b):

$$b_\ell = -\frac{i x_0^{-2} (\rho_0/\rho_1)}{h_\ell^{(1)}(x_0) j_\ell(x_1) - m_t j_\ell'(x_1) h_\ell^{(1)}(x_0)}, \quad (3a)$$

$$s_\ell = -\frac{j_\ell'(x_0) j_\ell(x_1) - m_t j_\ell(x_0) j_\ell'(x_1)}{h_\ell^{(1)}(x_0) j_\ell(x_1) - m_t j_\ell'(x_1) h_\ell^{(1)}(x_0)}. \quad (3b)$$

Both coefficients share the same denominator, which may vanish for special combinations of m , m_t , and x_0 . These divergences are also observed in far-field problems, particularly in the scattering field [24, 36]. Additionally, such a denominator can lead to resonance phenomena. At resonance, the system's energy becomes significantly amplified due to constructive interference, making energy analysis a valuable tool for detecting and characterizing these phenomena [37]. Thus, the energy of a system composed of an acoustic wave interacting with a scattering center is

$$W = \int_V \frac{|p(\mathbf{r}, t)|^2}{2 \rho_1 c_1^2} dV + \int_V \frac{\rho_1 |v(\mathbf{r}, t)|^2}{2} dV. \quad (4)$$

The Eq. (4) characterizes the transfer of energy by sound waves through a medium. The potential energy arises from pressure variations induced by the sound wave, which alternately compresses and rarefies the fluid. The kinetic energy is associated with the oscillatory motion of fluid particles driven by the passage of the wave. Using the internal scalar potential φ_1 from Eq. (2b), it is possi-

ble to explicitly calculate the potential and kinetic energy using Eq. (4). For the potential energy, the integral can

be solved analytically yielding

$$\frac{2f_0 W_K}{Z_1 |B|^2} = x_1^3 \sum_{\ell=0}^{\infty} |b_\ell|^2 (2\ell + 1) \left[\frac{\ell(2\ell + 1)}{x_1^3} I_1(x_1) - \frac{2\ell}{x_1^3} I_2(x_1) + \frac{1}{2} (j_{\ell+1}^2(x_1) - j_\ell(x_1) j_{\ell+2}(x_1)) \right], \quad (5a)$$

$$\frac{2f_0 W_P}{Z_1 |B|^2} = x_1^3 \sum_{\ell=0}^{\infty} |b_\ell|^2 (2\ell + 1) [j_\ell^2(x_1) - j_{\ell-1}(x_1) j_{\ell+1}(x_1)]. \quad (5b)$$

with frequency f_0 of the incident wave, and $I_1(x_1) = \int_0^{x_1} j_\ell^2(x) dx$, and $I_2(x_1) = \int_0^{x_1} j_\ell(x) j_{\ell+1}(x) x dx$. The value $(2f_0/Z_1|B|^2)$ normalizes the expressions for kinetic and potential energy, ensuring they are dimensionless. The integrals $I_1(x_1)$ and $I_2(x_1)$ lack an explicit analytical expression and thus must be calculated numerically. We truncate the summation of the partial-wave series at

$$\ell_{\max} = 3 + \left[x_0^{(\max)} + 4.05 \left(x_0^{(\max)} \right)^{1/3} \right], \quad (6)$$

following the numerical analysis in Ref. [38] to ensure the convergence in scattering calculations. The size parameter $x_1 = k_1 a$ dictates the number of partial waves required for accurate results. This formula accounts for higher-order contributions, such as leaky Lamb waves, and ensures both accuracy and efficiency in the series summation, particularly in cases involving complex resonances. In this analysis, $x_0^{(\max)} = 10$ was the largest value considered, providing a reference for the upper bound on the size parameter for the calculations.

III. RESULTS

Acoustic impedance is a property that measures the opposition a medium offers to the transmission of sound waves. High acoustic impedance results in more resistance to sound wave propagation, while low acoustic impedance allows sound to pass more easily. A severe impedance mismatch disrupts this energy exchange, reducing the chances of resonance. Therefore, in systems with highly varied impedance, resonance effects are typically minimal or absent altogether.

A. Systems with a impedance ratio $Z_1/Z_0 \ll 1$

The large difference in acoustic impedance between medium 0 and medium 1 significantly affects the energy

distribution inside the scatterer. Here, we study the potential and kinetic energies within the scattering center, using Eqs. (5a) and (5b), the spherical scattering center was represented by an air bubble - medium 1 (density $\rho_1 = 1.205 \text{ kg/m}^3$ and speed of sound $c_1 = 343 \text{ m/s}$) - immersed in seawater - medium 0 (the density $\rho_0 = 1024 \text{ kg/m}^3$ and speed of sound $c_0 = 1522 \text{ m/s}$). The interaction between acoustic waves and the penetrable scatterer is examined as a function of the dimensionless size parameter x_0 .

Fig. 1 compares the potential and kinetic energies as functions of the dimensionless size parameter x_0 for an air bubble immersed in seawater. Fig. 1 (top left) shows the energy behavior for $\ell = 0$, highlighting key resonance effects. Resonance occurs when an acoustic wave interacts with a scatterer at specific frequencies, causing constructive interference and a significant amplification of energy inside or around the scatterer. These resonance peaks represent points where the acoustic wave strongly interacts with the scatterer, leading to substantial energy deposition. Notably, a resonance peak appears at $x_0 \ll 1$, corresponding to the monopole mode. This peak arises even though the scatterer is much smaller than the wavelength of the incident wave, primarily due to the impedance contrast between the air bubble and the surrounding seawater. Fig. 1 (top right) display the results for a sum over multiple values of ℓ , truncated at the maximum value ℓ_{\max} as described by Eq. (6). This truncation effectively captures the resonance behavior without increasing computational complexity. As x_0 increases, both curves exhibit oscillations related to resonance peaks. These oscillations become smoother and less pronounced over time, indicating that the system's response is stabilizing.

Similarly, the potential energy within the scatterer, as shown in Fig. 2, exhibits sharp resonance peaks as a function of x_0 . For larger values of x_0 , higher-order modes of ℓ begin to resonate, creating a comb-like structure of peaks.

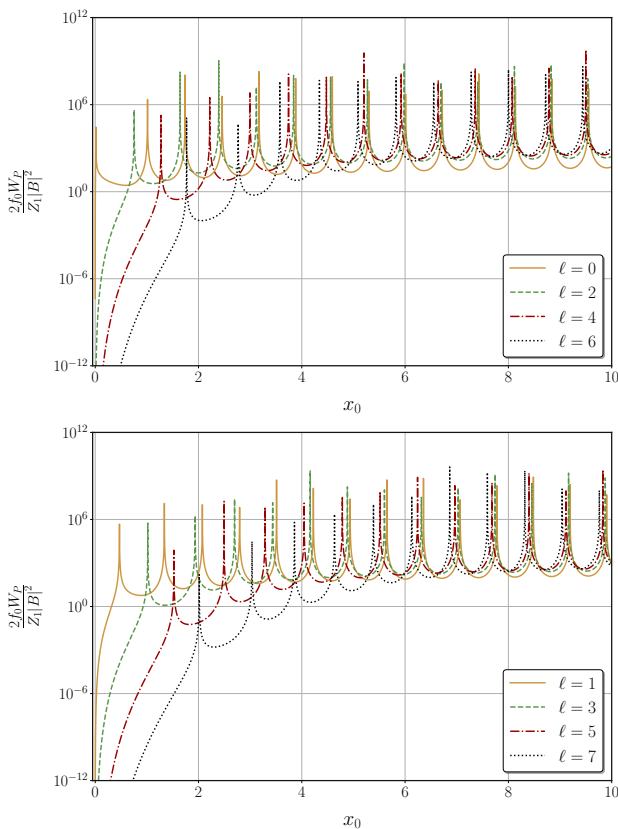


FIG. 2. Potential energy distribution, as a function of the dimensionless size parameter x_0 , for an air bubble (medium 1: $\rho_1 = 1.205 \text{ kg/m}^3$, $c_1 = 343 \text{ m/s}$) immersed in seawater (medium 0: $\rho_0 = 1024 \text{ kg/m}^3$, $c_0 = 1522 \text{ m/s}$). Separate plots are shown for even (top) and odd (bottom) values of ℓ . The resonance peaks, which grow in number as x_0 increases, indicate critical points where the acoustic wave is trapped and energy is deposited within the scattering center.

As x_0 increases further, the frequency of these peaks rises, indicating stronger resonance, as all modes interfere constructively when the scatterer approaches the wavelength size.

Likewise, the kinetic energy follows a similar trend, as shown in Fig. 3. Distinct resonance peaks appear as x_0 increases, with small-scale resonance clearly visible in the kinetic energy distribution, reflecting efficient energy transfer even for a small scatterer. As x_0 increases, the kinetic energy peaks across different values of ℓ become more synchronized. For $x_0 > 5$, the system reaches a regime where resonances align harmonically, suggesting strong and regular energy storage within the scatterer.

The existence of resonance behavior in Figs. 1, 2 and 3 for certain values of x_0 , representing combinations of the incident wavelength and particle radius, distinct peaks for both potential and kinetic energies are observed.

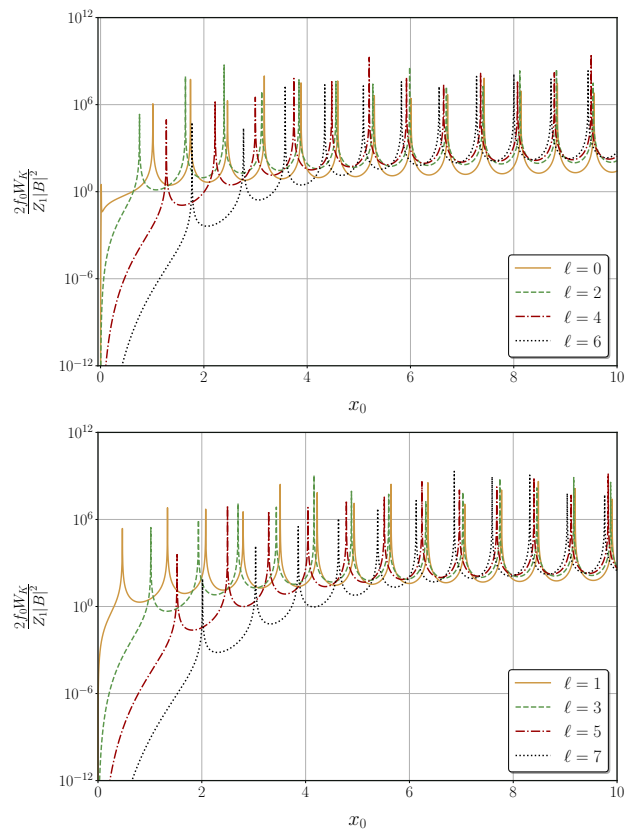


FIG. 3. The kinetic energy distribution as a function of the dimensionless size parameter x_0 for the air bubble in seawater. As with the potential energy, the resonance peaks reflect regions of high energy concentration within the scatterer.

These sharp peaks are unexpected in the small-particle regime, as resonance is typically associated with scattering centers of a size comparable to the incident wave.

$$\frac{2f_0}{Z_1 |B|^2} (W_K)_{\text{Small}} = \frac{m^5 x_0^5}{45} \left[\frac{m_t}{m} \frac{3}{(3 - m_t m x_0^2)} \right]^2, \quad (7a)$$

$$\frac{2f_0}{Z_1 |B|^2} (W_P)_{\text{Small}} = \frac{4m^3 x_0^3}{3} \left[\frac{m_t}{m} \frac{3}{(3 - m_t m x_0^2)} \right]^2. \quad (7b)$$

The presence of a single resonance peak at $x_0 \approx 0.014$ is revealed by Eq. (7), corresponding to the monopole mode ($\ell = 0$). This peak demonstrates that significant energy can be stored within the scattering center, even when the scatterer is much smaller than the wavelength of the incident wave. This unexpected result is due to the strong acoustic impedance mismatch between the air bubble and the surrounding seawater.

The results highlight pronounced resonance behavior, particularly in the small-sphere regime. Both potential and kinetic energies exhibit sharp peaks at specific values of x_0 , indicating significant resonance effects even when

the size of the scattering center is much smaller than the wavelength of the incident wave. This challenges the usual expectation that energy storage would be negligible in such a regime. The analysis confirms that resonance effects can still lead to substantial energy being stored within the scattering center, due to the strong acoustic impedance mismatch between the air bubble and the surrounding medium. As x_0 increases, higher-mode resonances become more frequent, leading to increased energy storage across different modes. These findings may enable the development of acoustic metamaterials

B. Systems with a impedance ratio $Z_1/Z_0 \approx 1$

In this section, we investigate the behavior of both potential and kinetic energies for a system comprising a petrol bubble submerged in seawater. The petrol bubble, with an acoustic impedance of approximately $968\,750\text{ kg/m}^2 \cdot \text{s}$, is immersed in seawater, whose impedance is around $1\,558\,528\text{ kg/m}^2 \cdot \text{s}$. This results in a moderate impedance ratio ($Z_1/Z_0 \approx 0.62$).

Fig. 4 illustrates the potential energy for both even and odd values of ℓ . Subfigure (a) displays the results for even ℓ values (0, 2, 4, 6), while subfigure (b) represents the odd values (1, 3, 5, 7). As x_0 increases, the curves for all ℓ values converge toward a stable potential energy. Notably, no significant resonance peaks are observed in either the even or odd modes, indicating a lack of strong energy trapping under these specific conditions. This absence of resonance suggests that the moderate impedance mismatch does not induce substantial energy localization within the scattering center.

Fig. 5 presents the kinetic energy for the same range of x_0 values, distinguishing between even and odd ℓ values. The trends mirror those observed in the potential energy curves, with kinetic energy remaining relatively stable, lacking pronounced oscillations or resonance peaks. Although minor fluctuations occur, the curves ultimately converge as x_0 increases.

For both potential and kinetic energy (see Figure 1 bottom), the absence of significant resonance peaks emphasizes the role of the impedance ratio in controlling energy distribution. The lack of pronounced energy localization for either even or odd ℓ values supports the conclusion that moderate impedance differences between media prevent strong resonance effects, which are typically observed when there is a larger contrast in acoustic properties.

The results presented in this section underscore the importance of parameter selection in the emergence of

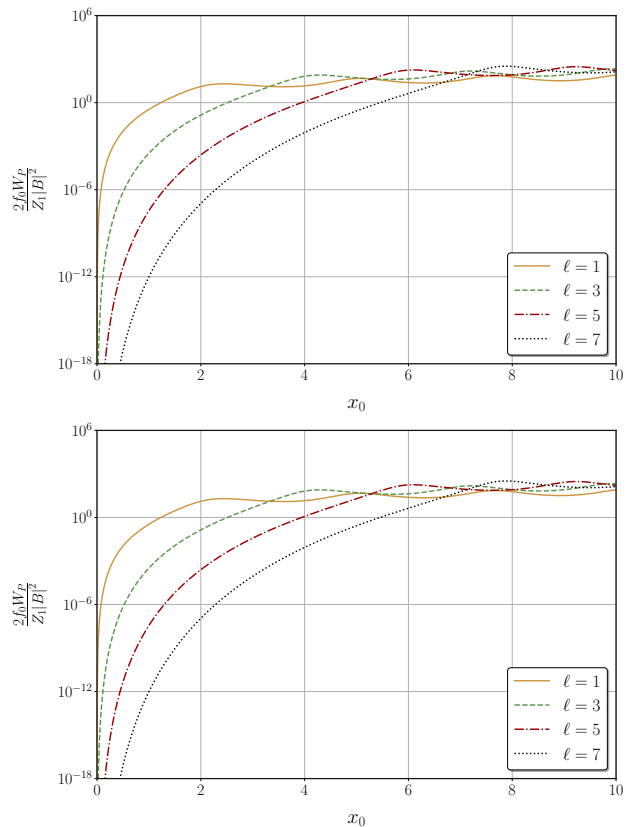


FIG. 4. Potential energy as a function of the dimensionless size parameter x_0 , is described by Eq. (5b), plotted separately for even ($\ell = 0, 2, 4, 6$) and odd ($\ell = 1, 3, 5, 7$). The petrol bubble ($\rho_1 = 968.75\text{ kg/m}^3$, $c_1 = 343\text{ m/s}$) is immersed in seawater ($\rho_0 = 1024\text{ kg/m}^3$, $c_0 = 1522\text{ m/s}$). No significant resonance peaks are observed.

resonance effects. The absence of distinct peaks in the energy distribution suggests that moderate impedance differences result in smooth, non-resonant energy behavior in acoustic scattering phenomena.

IV. CONCLUSION

In this study, we present an analytical approach to the single scattering of acoustic waves by spherical objects. We focus on the dynamics inside the scattering center through an energy analysis described by an internal wave, which is influenced by the internal and scattering coefficients. These coefficients exhibit divergences under specific combinations of media and scatterer parameters. These coefficient divergences are associated to wave resonances inside the scatterers. As a result, resonances may occur, even when the scatterer is much smaller than the wavelength of the incident wave, which was not expected.

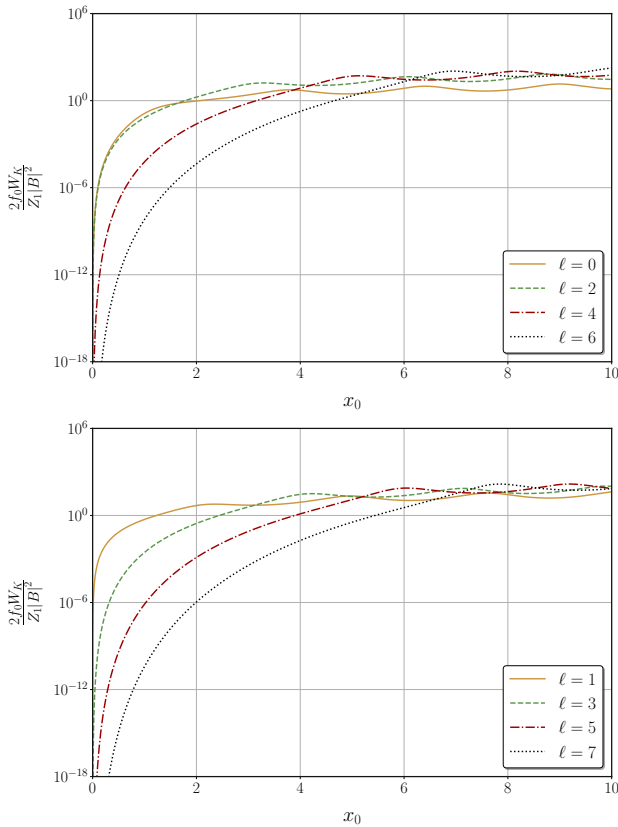


FIG. 5. Kinetic energy as a function of the dimensionless size parameter x_0 , is described by Eq. (5b), plotted separately for even ($\ell = 0, 2, 4, 6$) and odd ($\ell = 1, 3, 5, 7$). Similar to the potential energy, the petrol bubble ($\rho_1 = 968.75 \text{ kg/m}^3$, $c_1 = 343 \text{ m/s}$) in seawater does not exhibit significant resonance peaks, reflecting the system's moderate impedance ratio.

These resonance peaks, driven by the impedance mismatch between the scatterer and the surrounding fluid, lead to substantial energy storage, highlighting the importance of addressing even minor scattering effects to improve system efficiency and reliability. The framework developed here provides a foundation for further investigations into more complex scattering geometries, such as core-shell structures, where interactions between materials could enhance energy localization and control. Another approach is to explore multiple scatterers, non-ideal fluid dynamics, or non-linear effects. These developments would expand the model's applicability and deepen the understanding of wave scattering across diverse physical contexts. The insights gained from this work contribute to both the theoretical understanding of wave phenomena and practical applications, including the design of acoustic metamaterials [7, 15], soundproofing technologies [16], and virus deactivation [10].

ACKNOWLEDGMENTS

The authors gratefully acknowledge the financial support provided by the São Paulo Research Foundation (FAPESP) and the National Council for Scientific and Technological Development (CNPq). NER was supported by CNPq grant number 140549/2022-6; GN was supported by FAPESP grant 2023/07241-5; OMB thanks FAPESP by the grants 2018/22214-6, 2021/08325-2 and CNPq by the grant 307897/2018-4. ZRA was supported by FAPESP grants 17/09354-0 and 18/21694-4; ASM acknowledges the CNPq grant 0304972/2022-3. This support was essential for the successful completion of this research.

-
- [1] R. Newton, *Scattering Theory of Waves and Particles*, Dover Books on Physics (Dover Publications, 2002).
- [2] G. C. Gaunaurd and M. F. Werby, Acoustic Resonance Scattering by Submerged Elastic Shells, *Applied Mechanics Reviews* **43**, 171 (1990).
- [3] G. S. . G. G. Gurtainac, Acoustic resonance scattering of air bubbles in unbounded water, *Annals of the Academy of Sciences* **765**, 65 (1976).
- [4] E. L. Thomas, Bubbly but quiet, *Nature* **462**, 990 (2003).
- [5] R. S. D.-S. . K. R. Weitzinger, Sonoluminescence, *Annual Review of Fluid Mechanics* **42**, 231 (2010).
- [6] V. L. . A. Touin, Superabsorption of acoustic waves, *Applied Physics Letters* **99**, 1206 (2011).
- [7] A. Bretagne, A. Tourin, and V. Leroy, Enhanced and reduced transmission of acoustic waves with bubble metascreens, *Applied Physics Letters* **99**, 10.1063/1.3663623 (2011).
- [8] Y. Zhang, H. Wei, and H. Fang, Photoacoustic waves of a fluidic elliptic cylinder: Analytic solution and finite element method study, *Frontiers in Physics* **10**, 960165 (2022).
- [9] C. Stride and N. Staffin, Microbubble ultrasound contrast agents, *Nature* **445**, 450 (2000).
- [10] F. P. Veras, R. Martins, E. Arruda, F. Q. Cunha, and O. M. Bruno, Ultrasound treatment inhibits sars-cov-2 in vitro infectivity, *bioRxiv* <https://doi.org/10.1101/2022.11.21.517338> (2022).
- [11] W. L. Anderson, Sound scattering from a fluid sphere, *The Journal of the Acoustical Society of America* **22**, 420 (1950).
- [12] W. F. . C. Anderson, Reduced transmission of acoustic waves with bubble metascreens, *The Journal of the*

- Acoustical Society of America **106**, 535 (1999).
- [13] T. K. Stanton, Sound scattering by cylinders of finite length in fluid cylinders, *The Journal of the Acoustical Society of America* **83**, 55 (1988).
- [14] J. T. Farra, Sound scattering by solid cylinders and tubes, *The Journal of the Acoustical Society of America* **23**, 405 (1951).
- [15] G. S. Sammelmann, D. H. Trivett, and R. H. Hackman, The acoustic scattering by a submerged, spherical shell. I: The bifurcation of the dispersion curve for the spherical antisymmetric Lamb wave, *The Journal of the Acoustical Society of America* **85**, 114 (1989).
- [16] M. C. Junger, Sound Scattering by Thin Elastic Shells, *The Journal of the Acoustical Society of America* **24**, 366 (1952).
- [17] S. M. Ivansson, Sound absorption by viscoelastic coatings with periodically distributed cavities, *The Journal of the Acoustical Society of America* **119**, 3558 (2006).
- [18] R. D. Doolittle and H. Überall, Sound Scattering by Elastic Cylindrical Shells, *The Journal of the Acoustical Society of America* **39**, 272 (1966).
- [19] R. K. Johnson, Sound scattering from a fluid sphere revisited, *Acoustical Society of America Journal* **61**, 375 (1977).
- [20] C. M. Davis, L. R. Dragonette, and L. Flax, Acoustic scattering from silicone rubber cylinders and spheres, *The Journal of the Acoustical Society of America* **63**, 1694 (1978).
- [21] A. M. Gunderson, T. D. Daniel, P. L. Marston, and M. J. Isakson, Observation and modeling of acoustic scattering from a rubber spherical shell, *The Journal of the Acoustical Society of America* **143**, 3036 (2018).
- [22] S. Crampin, *The Excitation and Propagation of Elastic Waves* J. A. Hudson, Cambridge University Press, 1980 222 pp. £14.00, *Geophysical Journal International* **64**, 807 (1981).
- [23] G. Müller and M. Möser, eds., *Handbook of Engineering Acoustics*, 1st ed. (Springer, [S.l.], 2013).
- [24] W. C. Chew, Acoustic scattering by small particles: Lectures notes (2019), lecture 34 notes.
- [25] V. Sboros, K. V. Ramnarine, C. M. Moran, S. D. Pye, and W. N. McDicken, Acoustic rayleigh scattering at individual micron-sized bubbles, *Applied Physics Letters* **47**, 4287 (2002).
- [26] T. J. Arruda and A. S. Martinez, Electromagnetic energy within a magnetic infinite cylinder and scattering properties for oblique incidence, *J. Opt. Soc. Am. A* **27**, 1679 (2010).
- [27] T. J. Arruda and A. S. Martinez, Electromagnetic energy within magnetic spheres, *J. Opt. Soc. Am. A* **27**, 992 (2010).
- [28] T. J. Arruda, F. A. Pinheiro, and A. S. Martinez, Electromagnetic energy within coated spheres containing dispersive metamaterials, *Journal of Optics* **14**, 065101 (2012).
- [29] T. J. Arruda, A. S. Martinez, and F. A. Pinheiro, Unconventional fano effect and off-resonance field enhancement in plasmonic coated spheres, *Phys. Rev. A* **87**, 043841 (2013).
- [30] T. J. Arruda, F. A. Pinheiro, and A. S. Martinez, Electromagnetic energy stored in inhomogeneous scattering systems, *J. Opt. Soc. Am. A* **34**, 1934 (2017).
- [31] J. R. A. Alexandre Souto Martinez and T. J. Arruda, A set of basis functions to improve numerical calculation of mie scattering in the chandrasekhar-sekera representation, *Waves in Random and Complex Media* **31**, 2275 (2021), <https://doi.org/10.1080/17455030.2020.1738590>.
- [32] W. L. Anderson, Sound scattering by spheres in unbounded water, *The Journal of the Acoustical Society of America* **22**, 123 (1950).
- [33] P. M. Morse and K. U. Ingard, *Theoretical Acoustics* (McGraw-Hill, New York, 1948).
- [34] L. D. Landau and E. M. Lifshitz, *Fluid Mechanics* (Pergamon Press, Oxford, 1987) pp. 33–47.
- [35] G. B. Arfken and H. J. Weber, *Mathematical Methods for Physicists*, 7th ed. (Academic Press, 2012).
- [36] C. S. Clay and H. Medwin, Acoustic scattering: principles and applications, *ICES Journal of Marine Science* **60**, 563 (2003).
- [37] J. R. Alcarás, *Metamateriais acústicos: campos internos e teoria de espalhamento*, Phd thesis, Universidade de São Paulo, Faculdade de Filosofia, Ciências e Letras de Ribeirão Preto, Ribeirão Preto, SP, Brazil (2023), orientador: Alexandre Souto Martinez.
- [38] S. G. Kargl and P. L. Marston, Ray synthesis of the form function for backscattering from an elastic spherical shell: Leaky Lamb waves and longitudinal resonances, *The Journal of the Acoustical Society of America* **89**, 2545 (1991).